Biomimetic Spherical Silica Production using Phosphatidylcholine and Soy Lecithin

Ricky Curley[a,b], Russell A. Banta[a,b], Shane Garvey[a], Justin D. Holmes[a,b] and Eoin J. Flynn[b*]

[a] School of Chemistry & Tyndall National Institute, University College Cork, Cork, T12 YN60, Ireland.

[b] Amber Centre, Environmental Research Institute, University College Cork, Lee Road, Cork, T23 XE10, Ireland.

*To whom correspondence should be addressed: Tel: +353-21-490-1961; E-mail: eoin.flynn@ucc.ie

Keywords: Stöber process; biomineralisation; spherical silica; biomolecules; biomimetic synthesis

Abstract

Spherical silica particles are traditionally made via Stöber and modified-Stöber processes, which commonly use environmental toxins as reagents. Here we report a process to synthesise spherical silica particles using environmentally friendly biomolecules (phosphatidylcholine and soy lecithin) and employing water and soybean oil as solvents, rather than potentially harmful organic solvents. This scalable method represents an important step towards sustainable industrial silica syntheses. Under mildly acidic conditions phosphatidylcholine and soy lecithin can control the condensation of sodium silicate to form discrete, spherical silica particles. Silica particles with diameters ranging between 329 nm to 2232 nm were readily produced using phosphatidylcholine as the templating agent and soybean oil as the solvent in the presence of sodium silicate. Narrower size distributions (262 nm - 1272 nm) were achieved using soy lecithin as the templating agent in an aqueous acetate buffer solution containing sodium silicate. Silica particles grown using low concentrations of phosphatidylcholine and soy lecithin as templating agents formed by a combination of coalescence and Ostwald ripening, whilst particles grown at high concentrations predominantly formed through Ostwald ripening behaviour. The possibility of sustainably producing spherical silica particles in a simple biomolecule-templated synthesis is shown.

Introduction

Finding sustainable and environmentally friendly alternative routes to produce spherical silica is critical. Spherical silica particles are one of the most important and versatile mineral materials produced industrially with many integral uses in catalysis, adsorption, chromatography, sensors and drug delivery (Naderizadeh et al. 2018; Manzano and Vallet-Regí 2020; Sobańska 2020; Fragou et al. 2020). However, production of spherical silica currently relies on environmentally damaging and unsustainable processes (namely Stöber and modified-Stöber processes) which use ammonium hydroxide, quaternary ammonium surfactants, e.g., cetyltrimethylammonium bromide (CTAB), alcoholic solvents, and various alkoxysilanes. Ammonium hydroxide and CTAB control the morphology of the particles by acting as structure-directing agents (SDAs). However, these reagents have adverse environmental effects due to their toxicity (Nałęcz-Jawecki et al. 2003; Capello et al. 2007). Nevertheless, these SDAs are required to form spherical particles. Therefore, any sustainable process for producing spherical silica particles needs to address the inherent environmental issues of the Stöber processes while also maintaining the ability to control the morphology of the particles.

Biomineralisation, the process by which biological systems create complex, hierarchical, mineral structures, often out of silica, from simple starting materials may offer the solution to forming silica particles in an environmentally friendly way. The structures made by these organisms through biosilicification are quite extraordinary, and serve as inspiration for creating nanomaterials in similar ways (Wysokowski et al. 2018). Synthesis of bioinspired nanomaterials is a vibrant area of research (Gong et al. 2019; Perrett et al. 2019; Chen et al. 2019) and offers many opportunities to make current nanomaterial syntheses more sustainable. Within the natural World's producers of complex, hierarchical, silica structures, *diatoms* have been widely studied (Kolbe et al. 2020;

Soleimani et al. 2020; Heintze et al. 2020). These tiny creatures can create intricate cell walls made of silica arranged in highly ordered structures over a variety of scales, from nanometres up to several hundred microns (Lopez et al. 2006). Nanofabrication of silica in diatoms occurs under ambient conditions at slightly acidic pH and results from specific interactions between biomolecules and silicic acid derivatives (Sumper et al. 2003).

How these biomolecules exert such fine control over the biomineralisation process is still not fully understood. Isolation of biomolecules from diatoms revealed that there were specific biomolecules responsible for silica biomineralisation. Long-chain polyamines (LCPAs) and proteins such as silaffins and silicanin were among the first identified (Sumper and Kröger 2004; Pamirsky and Golokhvast 2013; Kotzsch et al. 2017). Other studies showed that peptides containing adjacent carboxyl- and amino-groups, which are present in these proteins play a significant role in silica formation via a charge relay effect (Wallace et al. 2009; Kuno et al. 2011; Murai et al. 2014). Many residues present in the proteins isolated from diatoms are also phosphorylated and this has also been shown to be integral to the silica biomineralisation process (Lopez et al. 2006; Kröger et al. 2014; Sprenger et al. 2018). Electrostatic interactions between the silicate species and the biomolecules allow for fine control over the rate of silica polymerisation and the resulting mineral structure. For more detailed descriptions of these interactions, the reader is directed to Mann (2001), Lechner and Becker (2015), and Patwardhan and Staniland (2019).

There have been numerous attempts to synthesise spherical silica biomimetically using simple biomolecules. Amino acids and polyamines have been extensively studied due to the discovery that such compounds play an integral role in silica biomineralisation *in vivo* (Masse et al. 2008; Ramanathan et al. 2011; Xia 2014; Tilburey et al. 2019; Tengjisi et al. 2021). However, many of these studies, while successfully employing biomimetic principles to synthesis silica, use

TEOS/TMOS, ammonia, or ethanol, which are not conducive to a sustainable synthesis. Furthermore, some use various polyamines and cyclic amines which are not naturally occurring and must be synthesised synthetically. The ultimate goal of synthesising silica biomimetically is to use renewable reagents and environmentally benign synthesis conditions. Naturally occurring biomolecules can provide this opportunity.

To date, there are fewer scientific reports on producing spherical silica particles from more complex biomolecules through methods that seek to mimic natural processes. Most studies using complex biomolecules have resulted in agglomerated and highly size-polydisperse and non-spherical particles (Coradin et al. 2002, 2003; Jia et al. 2004; Gautier et al. 2008; Demadis et al. 2009). Jackson et al. (2015) synthesised spherical silica particles with good monodispersity using bovine serum albumin (BSA), however polyethyleneimine (PEI) was used as an additive to achieve this. PEI has a poor toxicology profile and lacks degradability (Cho 2012), which means its use is not conducive to a sustainable synthesis.

These studies show that morphological control is possible with certain biomolecules depending on their physicochemical properties. These biomolecules can induce silica polymerisation while also controlling morphology. The role surfactants, such as CTAB, play in the condensation of silica has been thoroughly investigated (Alothman 2012; Yi et al. 2015; Hyde et al. 2016). They arrange themselves into micelles above the critical micelle concentration (cmc) and act as SDAs, controlling the silica particle morphology during synthesis. In traditional CTAB and tetraethyl orthosilicate (TEOS)-based modified-Stöber reaction systems, alcohol acts as a mutual solvent for both water and TEOS. Thus, hydrolysis and condensation of silica occurs at the shell of the SDA micelles. Once TEOS is hydrolysed, oligomeric silicate species are produced. These negatively charged species interact electrostatically with the positively charged quaternary ammonium SDAs

(Alothman 2012) and growth of the particles proceeds via aggregation and/or addition mechanisms. Electrostatic interactions mediate particle growth, while also preventing agglomeration of the particles, yielding discrete, spherical silica particles. Detailed discussions of the silica formation mechanism are provided elsewhere (Trinh et al. 2006; Rahman and Padavettan 2012; Han et al. 2017).

Using biomineralisation as a starting point, we identified phosphatidylcholine (PC) and soy lecithin (SL) as ideal candidates to replace CTAB in the Stöber processes. The phosphate group present in lecithin is structurally similar to the phosphoryl group present in biomineralising proteins. PC and SL also contain large hydrophobic tails of fatty acids and hydrophilic headgroups similar to CTAB. Specifically, the presence of quaternary ammonium cations in the headgroup of PC and SL, like CTAB, is important for morphological control. Soy lecithin is a waste product obtained from crude soy oil after degumming. Valorisation of waste streams is an important aspect of the circular economy aimed at reducing waste, while utilising renewable resources. This is in stark contrast to petrochemical surfactants such as CTAB, which are non-renewable and environmentally damaging. Furthermore, we use buffered media as the catalyst for hydrolysis, eliminating the need for ammonium hydroxide. The use of such biomolecules permits further reductions in the environmental impact of the Stöber silica production process, as such biomolecules can be processed using water-based chemistries and so permit the greatly reduced use of petrochemically derived solvents, which can be highly toxic, can damage environments and ecosystems, and come with large embedded environmental costs due to their methods of manufacture and source material, i.e., oil.

Experimental

Materials

Sodium silicate (10.6 % Na_2O, 26.5 % SiO_2) from Sigma Aldrich was used as the silicic acid source, as it is analogous to the natural form of soluble silica. Soy Lecithin (SL) was purchased from Modernist Pantry. Buffer solution was 0.05 mol L^{-1} acetate (pH 5.92) and was prepared in distilled water. L-α-Phosphatidylcholine (PC) (assay: ≥ 40 % phosphatidylcholine, TLC; ≥ phosphatides (as acetone insolubles)) and soybean oil were purchased from Sigma Aldrich.

Silica preparation using L-α-phosphatidylcholine and soy lecithin

Sodium silicate was added to 50 mL soybean oil under stirring. Aliquots of L-α-phosphatidylcholine stock solution (10 g L^{-1} of L-α-phosphatidylcholine in an aqueous solution of 0.05 mol L^{-1} acetate buffer, pH 5.92) were subsequently added. For preparation using soy lecithin, the procedure is similar except 50 mL acetate buffer (0.05 mol L^{-1}, pH 5.92) was used as the reaction medium and aliquots of soy lecithin stock solution (20 g L^{-1} soy lecithin in an aqueous solution of 0.05 mol L^{-1} acetate buffer, pH 5.92) were used. The reaction solution was stirred in a closed vessel at room temperature and left overnight. This solution was then centrifuged at 14,000 rpm in an Eppendorf® MiniSpin Plus microcentrifuge and washed with minimal water, ethanol, and acetone to remove any residual reactants. The sample was then dried. **Table S1** shows the experimental conditions for silica preparation using L-α-phosphatidylcholine and soy lecithin.

Characterisation

Scanning Electron Microscopy (SEM) was used to obtain images of the silica particles. SEM analyses were carried out on an FEI Inspect and Quanta 650, operated at either 10 or 15 kV. Each sample was adhered to a stainless-steel stub (stage) via double-sided carbon tape.

Elemental characterisation was acquired using energy-dispersive x-ray spectroscopy (EDX) on the FEI Quanta 650 instrument using Oxford Instruments INCA software. Particle diameters were determined using ImageJ image analysis software and statistical analyses were performed in OriginLab OriginPro 9.0 software.

Dynamic light scattering (DLS) measurements were conducted on a Malvern Panalytical Zetasizer Nano ZSP using non-invasive backscattering (NIBS) technology. The scattering angle was set at 173° and the measurement temperature was set to 20 °C. Samples were dispersed in ethanol and sonicated to give a stable solution prior to analysis.

X-Ray Photoelectron Spectroscopy (XPS) spectra were acquired on an Oxford Applied Research Escabase XPS 230 System equipped with a CLASS VM 100 mm mean radius hemispherical electron energy analyser with multichannel detectors in an analysis chamber with a base pressure of 5.0×10^{-9} mbar. A pass energy of 50 eV, a step size of 0.7 eV and a dwell of 0.3 s was used for survey spectra which were swept twice. All core level scans were acquired with a step size of 0.1 eV, a dwell time of 0.1 s and a pass energy of 20 eV averaged over 10 scans. A non-monochromated Al-Kα X-ray source (1486.58 eV) at 100 W power (10 mA, 10 kV) was used for all scans. All spectra were acquired at a take-off angle of 90° with respect to the analyser axis and were charge corrected with respect to the C 1s photoelectric line at 284.8 eV. Synthetic peaks are Gaussian in shape. The relative sensitivity factors used are from a CasaXPS library containing Scofield cross-sections. Nitrogen sorption measurements were performed on a Micromeritics TriStar II surface area analyser (Micromeritics, Norcross, GA, USA). Samples were pre-treated by heating at 200 °C under nitrogen for 12 hours. Surface area was measured using the Brunauer-Emmett-Teller (BET) method. Pore volume and pore diameter data was calculated using the

Barrett, Joyner and Halenda (BJH) method. Specific surface areas were calculated from the measured relative pressure in the range of P/P_0= 0.01 to P/P_0= 0.3.

Results & Discussion

Molecules like CTAB, which function as SDAs in modified-Stöber processes, produce spherical silica particles by forming micelles in the reaction solvent, with silica condensation occurring at the surface of the micelles followed by assembly of the micelles into larger structures. The SDA controls the rates of hydrolysis and condensation and controls the shape by adsorbing onto the surface of the growing particle. (Anderson et al. 1998; Slowing et al. 2010; Keane et al. 2010; Yi et al. 2015; Möller and Bein 2016). The long-chain, hydrophobic, hydrocarbon tail group combined with the charged headgroup of CTAB promotes micelle formation. Both PC and SL contain structural features akin to CTAB - hydrophobic, long-chain fatty acid residues, and quaternary ammonium headgroups, which are functionally similar to CTAB's head and tail groups. In the same way these properties enable CTAB to form micelles in solution, PC and SL can form similar bilayer structures (Murdan 2005; Shaikh et al. 2006; Galarneau et al. 2007; Cabezas et al. 2016). To test this, we obtained DLS data of PC and SL in solution. Dynamic light scattering (DLS) was used to analyse bilayer formation of PC and SL in the reaction solvent (aqueous solution of 0.05 mol L^{-1} acetate buffer at pH 5.92). **Fig. 1a** shows that PC forms possible bilayer aggregates at all concentrations tested in acetate buffer solution. Increasing the concentration of PC had little effect on the structure size. At all concentrations of PC, the peak 1 mean is relatively consistent (**Table S2**). Peak 2 is likely due to the formation of large aggregates/flocculates which commonly form in biomolecule solutions when they are sonicated (Lorber et al. 2012). However, the effect of these large aggregates on the determination of the structure size (peak 1) is negligible

at such low intensity. The polydispersity index (PDI) for each concentration also did change much (**Table S2**). The mean PDI for PC was 0.349.

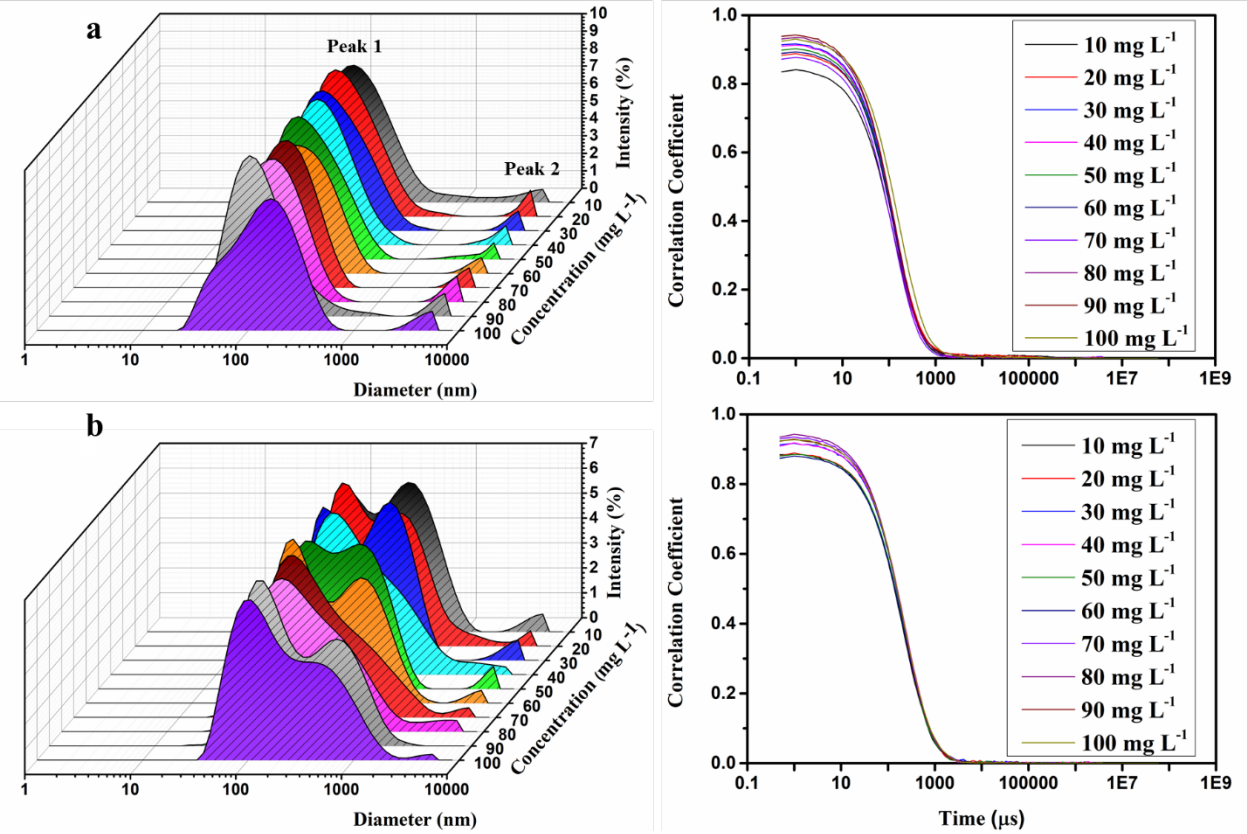

Fig. 1 PSD data and correlograms from DLS measurements of (a) phosphatidylcholine in acetate buffer (0.05 mol L^{-1}, pH 5.92) and (b) soy lecithin in acetate buffer (0.05 mol L^{-1}, pH 5.92) at various concentrations

Similarly, DLS data (**Fig. 1b**) shows that SL likely forms bilayer aggregates at all concentrations tested in acetate buffer solution. The PSD for SL in acetate buffer (**Fig. 1b**) shows a bimodal distribution which varies depending on concentration. **Table S2** shows how the peak means change with concentration. The average PDI is 0.423, which is higher than for PC in the same system and the same concentrations. In fact, **Table S2** shows that the PDI for SL is higher than that of PC at all concentrations. This difference in peak shape and PDI is expected because SL is less refined than PC and contains a higher number of different phospholipids. The greater variety of fatty acid

chain length contributes to larger variation if the aggregate size, hence higher polydispersity. **Fig S1** shows the structural similarities between lecithin and its derivatives, and CTAB.

Fig. S2 shows results from control experiments in which no PC or SL was used in the reaction system. In the absence of the biomolecules no spherical silica particles are formed, only unstructured monoliths. Based upon the results of these control experiments we could draw the following conclusions: (i) Spherical silica particles could not form under our proposed reaction conditions, without the presence of a structural directing agent in the reaction. (ii) CTAB is known to function as a structural directing agent for formation of silica particles and the shape of the particles is influenced by the CTAB micelles along with its quaternary ammonium headgroup. PC and SL both contain quaternary ammonium headgroups similar to CTAB. The presence of these groups has been shown to be integral in biomineralisation by catalysing and directing silica formation.

Silica Production via Phosphatidylcholine (PC)

To test the ability of SL to form spherical silica particles in our proposed process, we first performed syntheses using PC in soybean oil and buffered solution. Lecithin is a mixture phospholipids, containing mainly PC, phosphatidylethanolamine (PE), phosphatidylinositol (PI), minor compounds such as phosphatidic acid (PA), and other substances (triglycerides, carbohydrates, etc.) (Cabezas et al. 2009). PC is the lecithin component most structurally similar to CTAB. PC took the place of CTAB as the structure-directing agent. Sodium silicate, which undergoes hydrolysis under acidic conditions to form $Si(OH)_4$, was used as the silica precursor, and was chosen as it is water-soluble and a close analogue to natural silicates. In dilute solutions, silicic acid undergoes polymerisation and condensation to form silica particles (Coradin et al.

2003). Zwitterionic compounds, such as PC, can electrostatically interact with the negatively charged oligomeric silicate species formed upon hydrolysis of sodium silicate. Acetate buffer was used as the catalyst for hydrolysis, in place of ammonium hydroxide. Soybean oil was used as the reaction medium, in place of ethanol, in this first experimental iteration.

Spherical particles were successfully produced using PC (**Fig. 2**). Given the results of our control experiments without an SDA present, we can conclude that the spherical particles are due to the presence of PC in the system. At 20 mg L^{-1} PC, spherical particles were observed with some agglomeration present (**Fig. 2a**). At 100 mg L^{-1} PC, spherical particles were also observed but with increased agglomeration (**Fig. 2b**). At 200 mg L^{-1} PC, spherical particles were observed with no agglomeration (**Fig. 2c**). At 400 mg L^{-1} PC, spherical particles were observed with some agglomeration (**Fig. 2d**). From these observations, it is clear that 200 mg L^{-1} PC produced the most discrete particles.

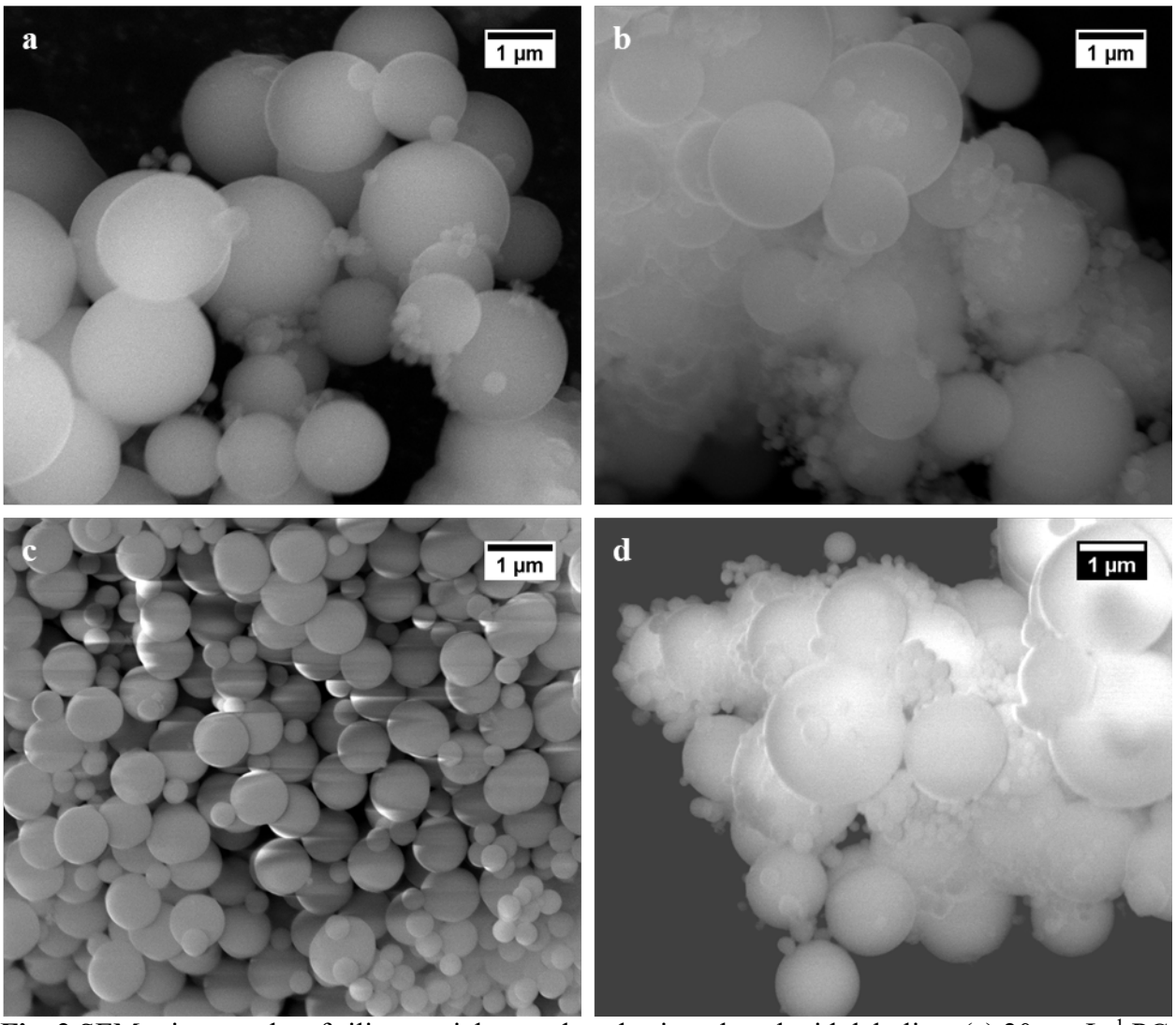

Fig. 2 SEM micrographs of silica particles produced using phosphatidylcholine. (a) 20 mg L^{-1} PC (PC1), (b) 100 mg L^{-1} PC (PC2), (c) 200 mg L^{-1} PC (PC3), and (d) 400 mg L^{-1} PC (PC4). All reactions done in 50 mL soybean oil with 500 µL sodium silicate at room temperature. Scale bars are 1µm

PSDs obtained when using PC (**Fig. 3**) show that the silica particles formed were polydisperse (multiple peaks). **Fig. 3a** shows a relatively broad particle size range and three distinct, widely separated, peaks at 329 nm, 1326 nm, and 2132 nm at 20 mg L^{-1} PC. Note also that **Fig. 3a** exhibits log-normal characteristics at small diameters, indicating coalescence at 20 mg L^{-1} PC. Coalescence is the fusion of smaller particles to form larger particles, resulting in a reduction in surface energy. Larger particles have a lower, stabler, more favoured energy state than smaller

particles and this is what drives the process. Coalescence can be identified in the PSD by a log-normal distribution. Combination of particles of different sizes to form particles of larger size results in right-skewed distribution, *i.e.*, log-normal. Increasing PC concentration from 20 mg L^{-1} to 100 mg L^{-1} (**Fig. 3b)** results in an increase in particle diameter and polydispersity, represented by an increase in number of peaks at 100 mg L^{-1} PC (6 peaks) in comparison to 20 mg L^{-1} PC (3 peaks). These six peaks at 100 mg L^{-1} PC are at 380 nm, 557 nm, 886 nm, 1407 nm, 1730 nm, and 2232 nm. This wide range of diameters, indicates decreased morphological control, resulting in high polydispersity at 100 mg L^{-1} PC. Further increasing the concentration of PC to 200 mg L^{-1} sees a reduction in size range and in the number of peaks observed (3 peaks) (**Fig. 3c**) indicating greater control of particle size at this PC concentration. These three peaks have means of 344 nm, 618 nm, and 849 nm. These peaks at 200 mg L^{-1} PC are similar to those observed at 100 mg L^{-1} except the peaks at the larger diameter (1407 nm, 1730 nm, and 2232 nm) disappear, suggesting that PC is exerting greater morphological control at 200 mg L^{-1} than 100 mg L^{-1}. Increasing PC concentration further still, to 400 mg L^{-1} (**Fig. 3d**), the number of peaks increases to four (161 nm, 299 nm, 1353 nm, and 1589 nm). However, the FWHM of these peaks also decreases significantly, indicating that the polydispersity at these peak diameters has decreased. These changes in particle size and polydispersity broadly correlate with the DLS data. **Fig. S3** shows how the Z-average diameter of the bilayer structure changes with concentration of PC. At 20 mg L^{-1} PC the mean diameter is 95nm, at 100 mg L^{-1} it is 115nm, at 200 mg L^{-1} it is also 115nm, and at 400 mg L^{-1} it is 116 nm. **Fig. S4** shows how the PDI changes with concentration. At 20 mg L^{-1} the PDI is 0.357, at 100 mg L^{-1} it is 0.394, at 200 mg L^{-1} it is 0.388, and at 400 mg L^{-1} it is 0.397. While the Z-average diameter increases with increasing PC concentration, this increase may be a result of aggregation or flocculation of PC at higher concentrations. Accordingly, it is difficult to determine

whether this has any significant effect on particle size. Though, higher concentrations of PC do seem to reduce the level of polydispersity of the particles.

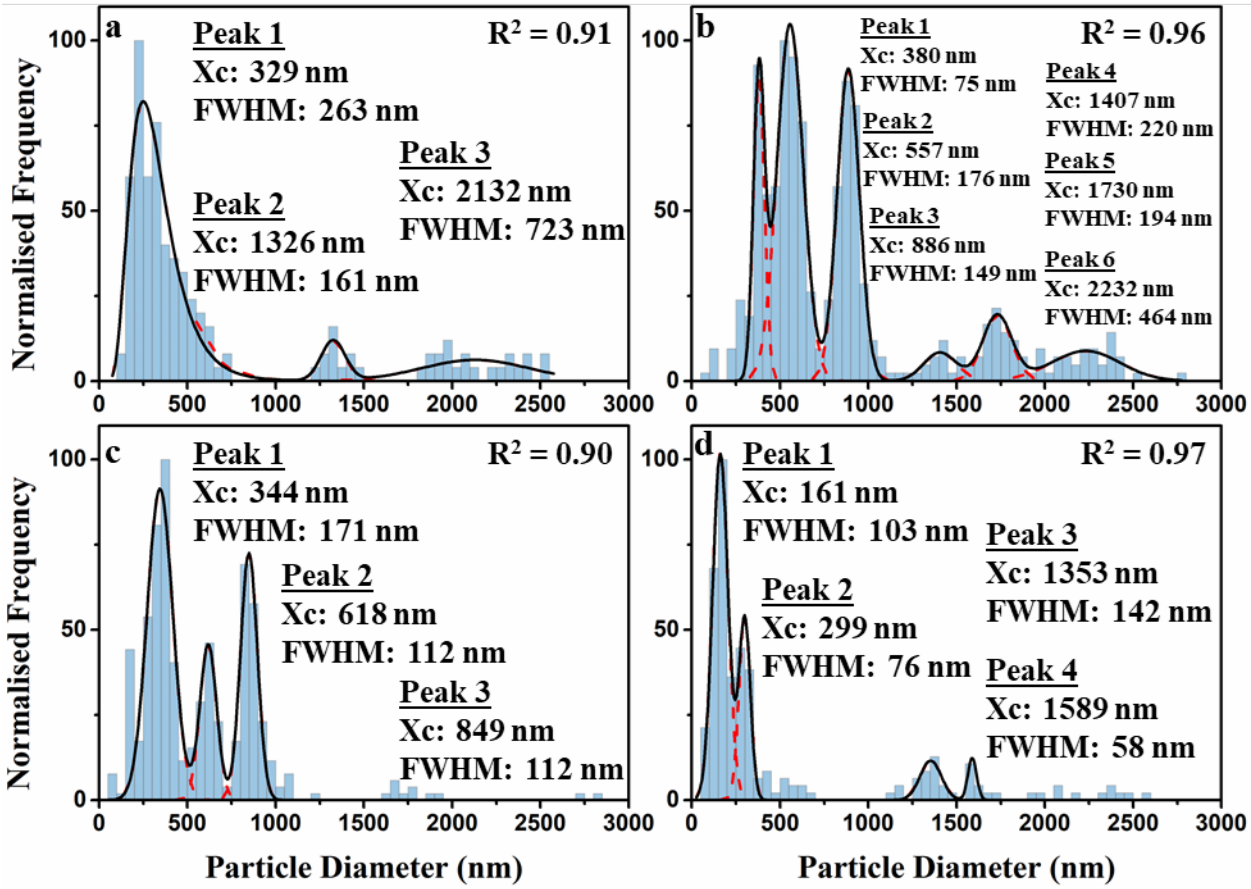

Fig. 3 PSDs of silica particles produced when using PC (a) 20 mg L^{-1} PC (PC1), (b) 100 mg L^{-1} PC (PC2), (c) 200 mg L^{-1} PC (PC3), and (d) 400 mg L^{-1} PC (PC4). All reactions done in 50 mL soybean oil with 500 µL sodium silicate at room temperature

Fig. 3d also gives a clear indication that Ostwald ripening is occurring. The peaks on the smaller diameter side shift left, while larger particles over 1350 nm begin to emerge. Ostwald ripening is the growth of large particles at the expense of smaller particles, rather than a fusion of smaller particles, which occurs due to the unfavourably high surface energy increase associated with the phase transition from homogenous solution to solid particle (Santos et al. 2017). To minimise this surface energy increase, smaller particles redissolve, and reactive units (either monomers or small

aggregates) diffuse to the surface of larger particles to continue growth. A mathematical description of Ostwald ripening called the *LSW model* was given by Lifshitz and Slyozov (1961) and Wagner (1961). Using the precepts of this model it is possible to determine which of the growth processes, coalescence or Ostwald ripening, is the dominant one by examining PSDs (Banta et al. 2018). Ostwald ripening occurs via the transfer of material from smaller particles to larger particles. Thus, the LSW model produces a characteristic left-skewed distribution,. One of the assumptions of the LSW model is that the solution is infinitely dilute. A consequence of this is that particle interaction is absent from the model and no particle greater than 1.5 times the mean particle diameter can exist. Thus, to account for particle interaction, the LSW model must be modified, and a Gaussian fit provides a better description (Ma and Ardell 2007; Lotty et al. 2013; Santos et al. 2017), which is precisely what we applied to our own data. Insights into the growth mechanism of silica particles can be gleaned from examination of the PSDs obtained. Post nucleation, particle growth typically occurs by Ostwald ripening and coalescence processes. There is no acute distinction between coalescence and Ostwald ripening. Both processes coexist and overlap during particle formation. By understanding how changes in experimental conditions affect particle growth processes, particularly the extent to which coalescence or Ostwald ripening dominate, one can optimise a synthesis. Depending on which growth process dominates, the monodispersity of the final particles can be positively or negatively impacted.

One possible explanation of the data shown in **Fig. 3** is that at low PC concentration, a mixture of coalescence and Ostwald ripening occurs, indicated by the presence of both log-normal and Gaussian peaks. However, at higher concentration, Ostwald ripening appears to become the dominant process, as indicated by the presence of Gaussian peaks. The data indicate that when transitioning from a mixed (coalescence and Ostwald ripening) growth process to one dominated

by Ostwald ripening, the system undergoes a brief period of instability (**Fig. 3b**). This transition is characterised by maxima in polydispersity and particle size range. Although the spherical morphology of the particles is still maintained, indicating that PC is continuing its SDA role, the growth mechanics are not as well defined. Transition to a growth mechanism dominated by Ostwald ripening at high PC concentrations means better control of polydispersity. This is seen in the Gaussian distributions and narrow peak size (**Fig. 3c** and **d**). As outlined above, this Gaussian distribution is preferable to a log-normal (coalescence) one that skews to larger diameter. Thus, we can possibly optimise monodispersity and size range with high PC concentration.

Silica Synthesis via Soy Lecithin

Next, we investigated whether SL - the less refined source of PC – could function as an SDA and produce spherical particles. SL would be a more sustainable SDA to use because it requires less processing than PC. It is commonly used as a food additive and is readily available and inexpensive. Furthermore, the physicochemical properties of SL, such as its ability to form bilayers and its structural similarities to CTAB, make it a prime candidate as an SDA in sustainable spherical silica synthesis. Based on our results with PC - the major, CTAB-like component of SL - we expected that spherical silica particles could also be formed using SL. However, to increase the sustainability of our process, soybean oil was no longer used as the reaction medium as its production has its own associated environmental costs. Instead, the ability of SL to form spherical particles in aqueous acetate buffer was investigated.

Fig. 4 shows that spherical particles were successfully produced using SL. Given the results of our control experiments, we can conclude that the spherical particles are due to the presence of SL in the system. At 4 mg L^{-1} SL, spherical particles were observed with some agglomeration present

(**Fig. 4a**). At 40 mg L^{-1} SL, spherical particles were also observed with agglomeration (**Fig. 4b**). At 80 mg L^{-1} SL, spherical particles were observed with some agglomeration (**Fig. 4c**). At 1800 mg L^{-1} SL, spherical particles were observed with no agglomeration (**Fig. 4d**). From these observations, it is clear that 1800 mg L^{-1} SL produced the most discrete particles. It is worth noting however, that the quality of the particles is still something to be improved upon.

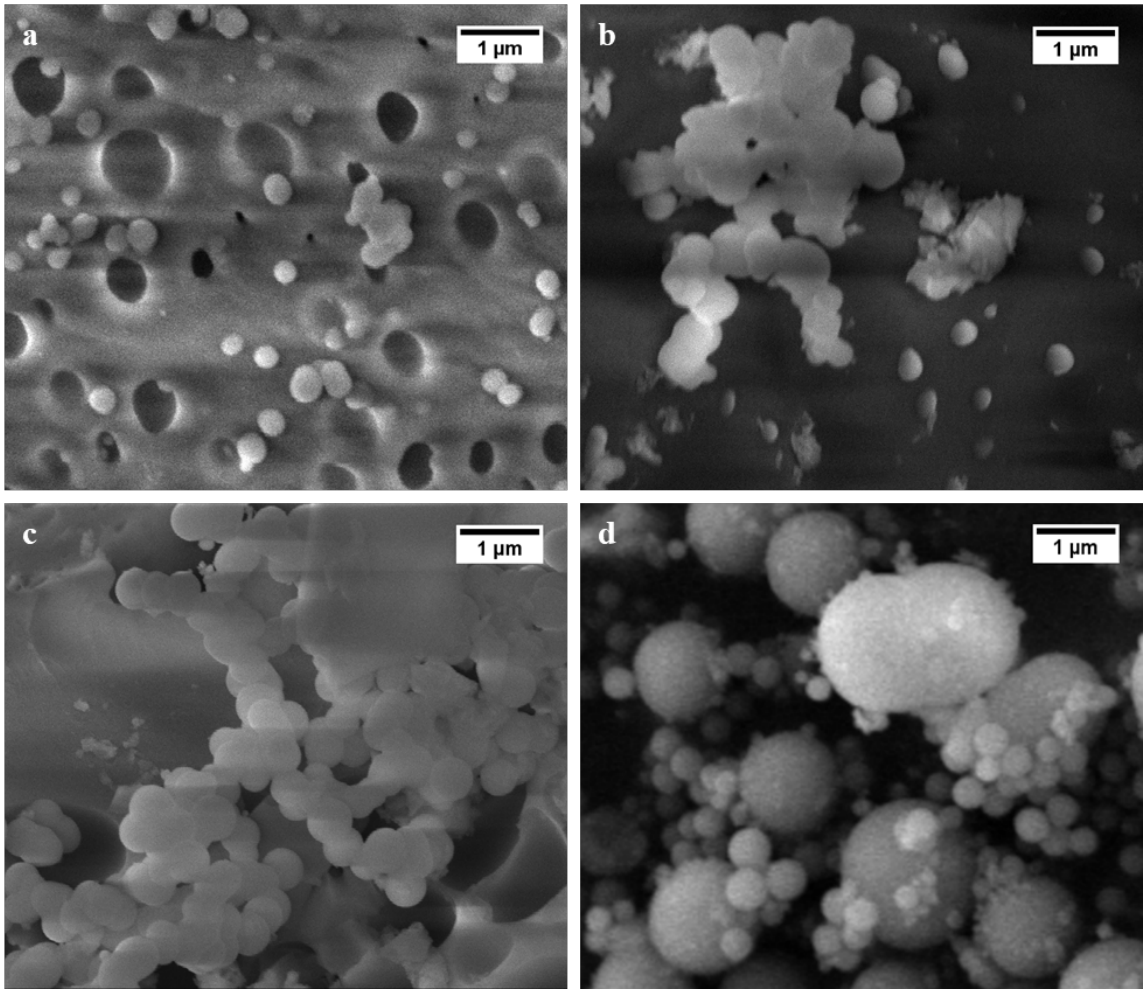

Fig. 4 SEM micrographs of silica particles produced when using SL with various aliquots of SL (a) 4 mg L^{-1} SL (SL1), (b) 40 mg L^{-1} SL (SL2), (c) 80 mg L^{-1} PC (SL3), and (d) 1800 mg L^{-1} SL (SL4). All reactions done in 50 mL acetate buffer (0.05 mol L^{-1}, pH 5.92) with 820 µL sodium silicate at room temperature. Scale bars are 1µm. Background in (a) is carbon tape

PSDs of these particles were lower and had narrower size ranges, mostly below 1000 nm (**Fig. 5**), in comparison to silica particles produced by PC. This is seen in the PSDs, where fewer peaks are present. Increasing the amount of SL from 4 mg L^{-1} to 40 mg L^{-1} shifts the PSD to larger diameter while also increasing the size polydispersity (**Fig. 5a** and **b)**. **Fig. 5a** shows a unimodal distribution with Gaussian fitting (R^2 = 0.97) with a mean particle diameter of 262 nm (4 mg L^{-1} SL). **Fig. 5b** shows a peak with a shoulder fitted with a combination of log-normal and Gaussian curves (R^2 = 0.75). Fitting log-normal or Gaussian alone results in a lower R^2 value. Peak 1 has a mean of 302 nm and peak 2 has a mean of 550 nm (40 mg L^{-1} SL). This suggests the onset of Ostwald ripening because there is a shift from a log-normal to a Gaussian distribution, while also resulting in a shift to larger diameter and an increase in small particles. A further increase in the amount of SL shifts the PSD to larger diameter with a decrease in polydispersity and a unimodal distribution with Gaussian fitting (R^2 = 0.97) with mean of 496 nm (80 mg L^{-1} SL, **Fig. 5c**). Increasing the SL concentration to 1800 mg L^{-1} results in two peaks with Gaussian fitting (R^2 = 0.97) with means 342 and 1272 nm (**Fig. 5d**). This shift to smaller diameters and the emergence of a peak at 1272 nm suggest Ostwald ripening is taking place (Lotty et al. 2013). This trend of increasing particle size with increasing SL is similar to that seen when using PC. However, compared to the increases with PC, they are not accompanied by large increases in polydispersity, and while the particle size generally increases with SL concentration, the size range reduces to a substantially narrower range than seen for PC.

Overall, the data suggest that coalescence and Ostwald ripening are both occurring (**Fig. 5b**). However, at higher SL concentrations the growth process transitions to one dominated by Ostwald ripening. This is comparable to the growth dynamics seen when using PC. However, the drastic transition from a mixed (coalescence and Ostwald ripening) growth process, with high

polydispersity and wide particle size range, to an Ostwald ripening dominated process is not seen when using SL. This suggests that using SL grants greater control over particle growth dynamics. This is evident in the improved monodispersity of the particles produced in the SL system (**Fig. 5**). Thus, SL produced particles which are smaller, and more size monodisperse than those produced using PC. Moreover, as observed in the PC experiments, at all concentrations of SL used spherical particles were obtained.

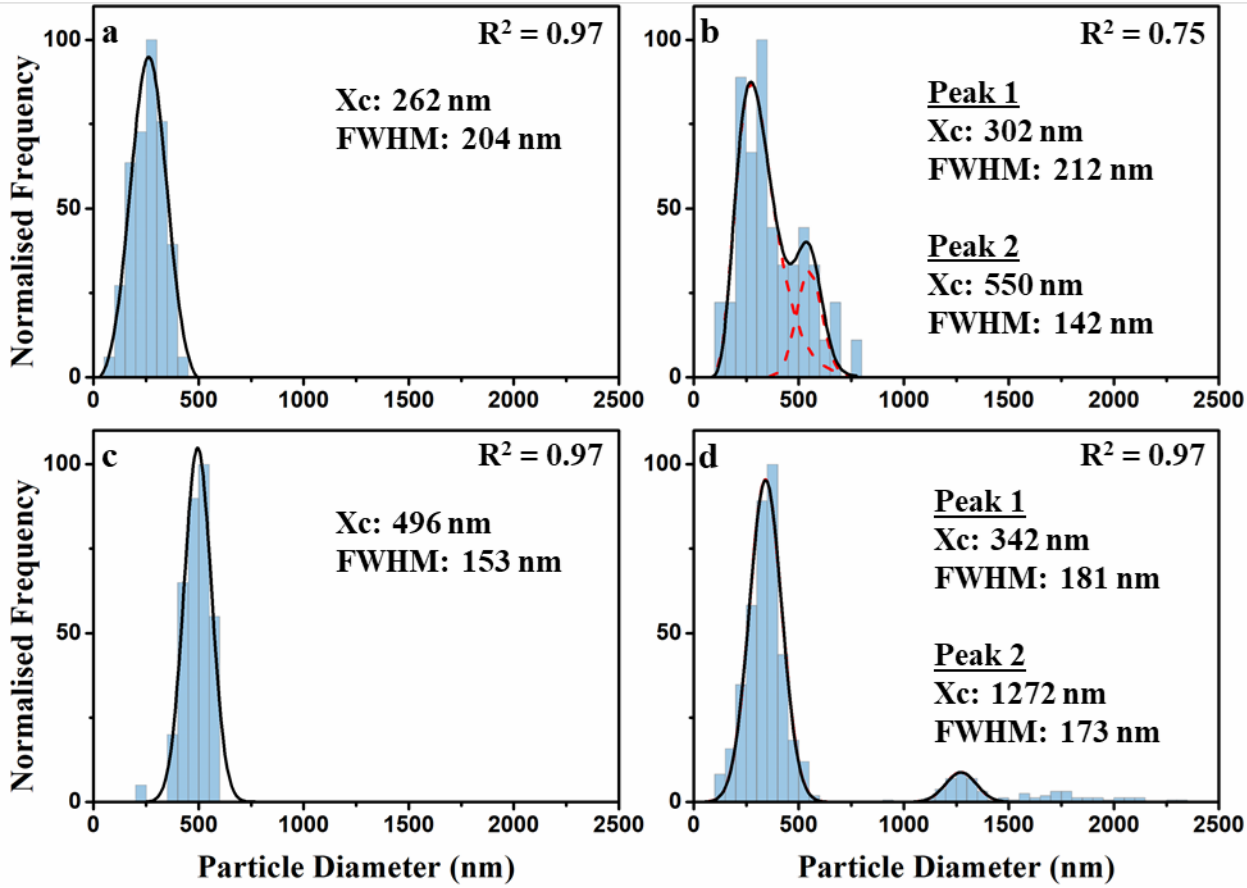

Fig. 5 PSDs of silica particles produced using soy lecithin (a) 4 mg L^{-1} SL (SL1), (b) 40 mg L^{-1} SL (SL2), (c) 80 mg L^{-1} SL (SL3), and (d) 1800 mg L^{-1} SL (SL4). All reactions done in 50 mL acetate buffer (0.05 mol L^{-1}, pH 5.92) with 820 µL sodium silicate at room temperature

Fig. S5 shows the nitrogen sorption isotherm and the pore size distribution of silica particles prepared with 80 mg L^{-1} SL (SL3). The isotherm is a Type H4 hysteresis loop, which is indicative of a mixture of both micropores and mesopores (Thommes 2010). This is also confirmed in the pore size distribution, which shows pore sizes of 17 and 39 Å. Removal of CTAB post-synthesis in a typical modified-Stöber process results in porous silica particles. Similarly, in our system, removal of SL post-synthesis also results in porosity.

Fig. 6a(i) shows the EDX spectrograph of the spherical particles from PC2 (100 mg L^{-1} PC), confirming the presence of silicon in the sample. **Fig. 6a(ii)** shows the EDX spectrograph of the spherical particles from SL4 (1800 mg L^{-1} SL), confirming the presence of silicon in the sample. Oxygen and carbon peaks are also present, although these are common contaminants in EDX spectra. To confirm that these particles were SiO_2, XPS analysis was performed. **Fig. 6b** shows the XPS spectra for PC2 (100 mg L^{-1} PC). **Fig. 6c** shows the XPS spectra for SL4 (1800 mg L^{-1} SL). The O 1s spectra show peaks at binding energies of 532.8 eV and 533.5 eV for PC2 (**Fig. 6b(i)**), and 532.9 eV and 533.7 eV for SL4 (**Fig. 6c(i)**), which correspond to Si-O-Si and Si-OH, respectively (Hollinger and Himpsel 1984; Himpsel et al. 1988; Gustus et al. 2014; Post et al. 2018). The small intensity peaks at 531.2 eV and 531.4 correspond to either C-O or C=O, but distinction between the two is not possible as the binding energies are closely related (Wang et al. 2014; Sadri et al. 2017). This peak is likely due to the presence of carbon contamination during the XPS analysis or small amounts of SL remaining in the particles. The sample was washed with water, ethanol, and acetone post-synthesis so that as much residual acetic acid, soybean oil, PC, and sodium acetate as possible is removed in this step. Thus, most residual carbon-containing compounds are removed from the particles. The peaks at 534.3 eV and 535.2 eV corresponds to O-H which is due to water contamination (Bebensee et al. 2008), or O-H on the silica surface. The

Si 2p spectra show two peaks corresponding to Si-O-Si and Si-O-H, which are indicative of SiO_2 (Yang et al. 2018; Post et al. 2018). Overall, the EDX and XPS data confirm that the particles are made of SiO_2.

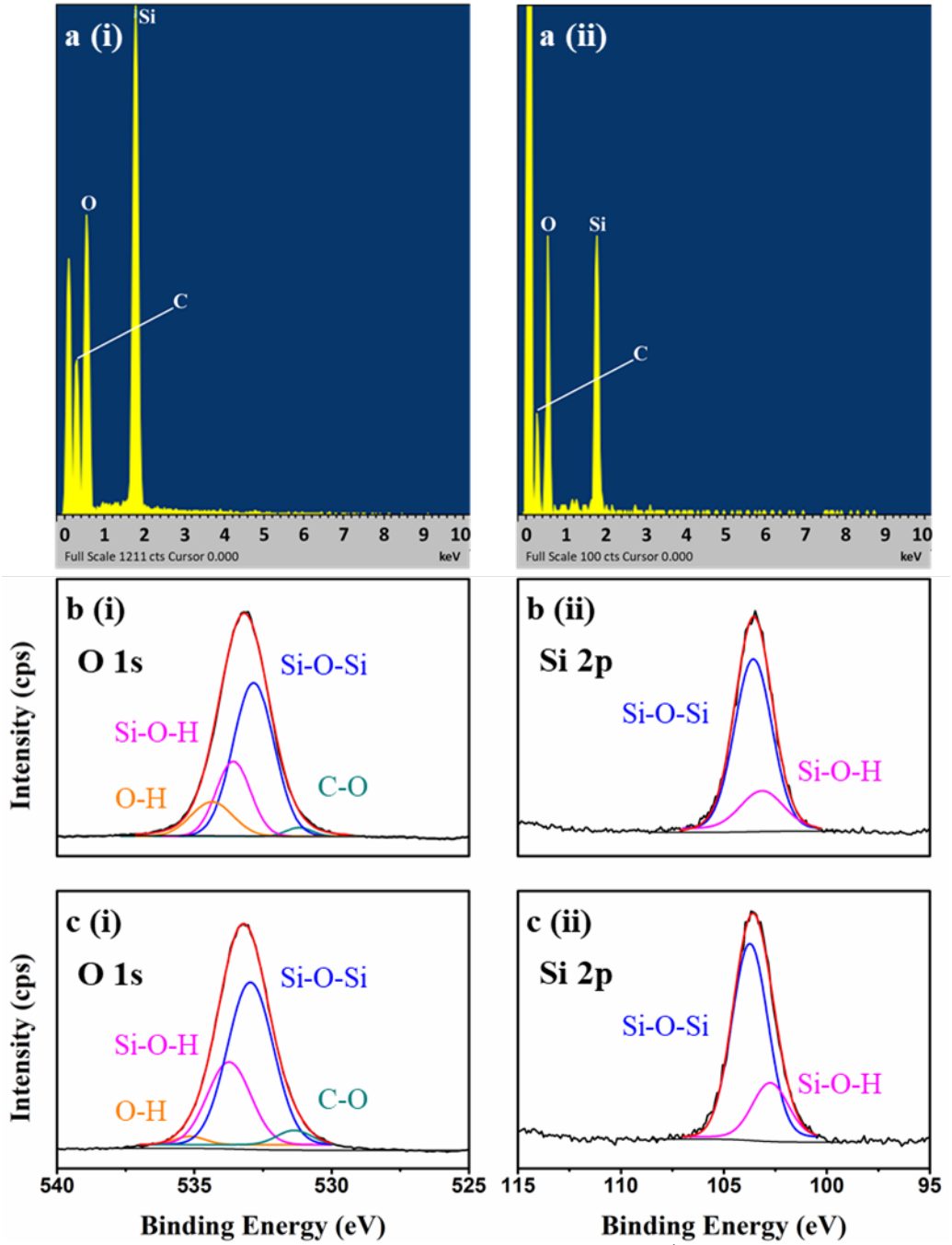

Fig. 6 Energy-dispersive x-ray spectra (a(i)) of PC2 (100 mg L^{-1} PC), and (a(ii)) SL4 (1800 mg L^{-1} SL), (b) XPS spectra of O 1s and Si 2p peaks of PC2 (100 mg L^{-1} PC). Red curve is the cumulative fitting, and (c) XPS spectra of O 1s and Si 2p peaks of SL4 (1800 mg L^{-1} SL). Red curve is the cumulative fitting

SL produced smaller, more size monodisperse silica particles than PC in our sustainable, biomolecule-based, modified-Stöber synthesis. Whereas the particle sizes of the silica produced using PC broadly correlated with the DLS data for PC, the particle sizes of the silica produced when using SL did not. Based on our initial DLS data, it was expected that SL would produce larger and more polydisperse silica than PC. However, SL produced smaller and more monodisperse particles than PC. To investigate this, we analysed the bilayers formed in our reaction system using SL with our silica precursor (sodium silicate) present. **Fig. S6** shows the temporal evolution of the mean diameter and PDI after sodium silicate addition. As time increases, the PDI decreases and the distribution becomes unimodal. The Z-average remains consistent over this time period. Our results, shown in **Fig. S7**, show that the presence of sodium silicate reduced the size of the SL bilayer structures while also narrowing their size distribution. One possible explanation for this is that the sodium ions from the sodium silicate co-localise with the ester moeity of the phospholipids (Le et al. 2019). This penetration of the sodium ion into the headgoup double layer enhances the attractive forces between the headgroups, likely leading to a change in curvature and reduction in size. This effect is likely happening in the PC system also, but to a lesser extent as there is little difference between the particle sizes observed with PC and the bilayer structure size of PC without sodium silicate. Addition of sodium silicate to SL in acetate buffer results in a smaller bilayer structure size than without sodium silicate, precisely as seen in our DLS data, which in turn results in a smaller than initially anticipated silica particle size.

The reason PC and SL are effective at producing spherical silica, is because modified-Stöber processes have been developed using long-chain quaternary ammonium surfactants, of which CTAB is an example (Prasomsri et al. 2015; Möller and Bein 2016). SL's mixture of phospholipids

(specifically PC) possessing quaternary ammonium cations and fatty acid residues, allow both SL and PC to behave like CTAB. Further understanding of the efficacy of our chosen biomolecules in modified-Stöber silica syntheses can be derived from studying natural silica formation. In diatoms, long-chain polyamines (LCPAs) and proteins such as silaffins and silacidins have been shown to be integral to silica formation. The LCPAs typically have a quaternary ammonium group and have been shown to have direct involvement in the structure-directing step in the biomineralisation process (Lechner and Becker 2015). Silaffins are proteins which possess these LCPAs and also have a high degree of phosphorylation and quaternary ammonium structures. Indeed, phosphorylation present in silaffins has been shown to be intimately involved in the biomineralisation process, promoting silica polymerisation through electrostatic and hydrogen-bonding interactions (Sprenger et al. 2018). These proteins bear similar structures to PC and SL (Kröger et al. 2014). These similarities are likely the reason PC and SL can form spherical silica particles in our system. Furthermore, silaffins and silacidins have been shown to induce silica polymerisation under acidic conditions in vitro (Wenzl et al. 2008; Kröger et al. 2014). To have the ability to both induce silica polymerisation (nucleation) and control its final structure (growth) means the catalyst typically required in the modified-Stöber synthesis is no longer required. The biomolecules, PC and SL, in our synthesis also have this functionality.

Regardless of the growth process, the monodispersity of the final sample is most important. Monodisperse particles are needed for advanced applications such as chromatography and drug delivery. A useful numerical descriptor of monodispersity is relative standard deviation (RSD) The lower this number, the more monodisperse the particles. **Table 1** shows a comparison of the best RSD of our results (SL3; 80 mg L^{-1} SL) to twelve other studies which explicitly state they have prepared monodisperse, spherical silica particles, using traditional syntheses, and four studies

using biomolecules to produce silica. Other studies that synthesised silica particles biomimetically using simple molecules such as amino acids and polyamines were not included, as a direct comparison between studies that use more complex biomolecules is prudent. The lowest RSD seen was 1.2 % and the highest was 59.8 %. Our RSD value of 13.1 % compares favourably with the monodispersity of silica particles prepared with traditional methods in the literature. Three of the biomolecule-based silica syntheses produced non-spherical particles and did not give any standard deviations, thus RSD calculation was not possible. The particles produced using our simple biomolecule-templated approach are discrete and exhibit moderate monodispersity.

We have shown that it is possible to synthesise spherical silica particles more sustainably than the Stöber processes. It is envisaged that such approaches will replace the current synthesis pathways, especially on a larger scale. However, the work detailed here is only a tentative step in this direction and there are some hurdles that need to be overcome before this can take place. Firstly, as is the case with many biomimetically-synthesised silica particles, the quality in terms of monodispersity is still below that of those synthesised via traditional means. This is a property that needs to be addressed before such biomimetic particles can compete with those produced via the Stöber processes. Secondly, the adoption of water-based chemistries at large scale is not widespread. Water has a high enthalpy of vaporisation, making its recovery and purification costly. Organic solvents on the other hand are much easier to recover and purify, and with the infrastructure to do so already in place, their use remains persistent. However, this problem is easily solved with investment in municipal and industrial water treatment and processing, which would reduce the need for organic solvents. The reduction in greenhouse gas emissions by switching to water-based chemistries would far outweigh the initial capital expenditure cost of setting up such treatment and processing infrastructure. Furthermore, use of renewable

biomolecules such as soy lecithin from valorised waste streams along with water-based chemistries reduces the embedded costs associated with petrochemical production and refinement. As long as obtaining biomolecules from such waste streams does not lead to maintenance of damaging industries that would otherwise fail economically without such valorisation, their use presents an opportunity to develop truly sustainable syntheses. Of course, regular life-cycle analyses would need to be conducted alongside any process which aims to adhere to the principles of green chemistry and the circular economy to ensure the process presents a positive improvement in sustainability. Such processes need to be developed because human-driven climate change is a real and present problem that needs to be addressed. The work detailed here showing that spherical silica particles can be produced sustainably using simple biomolecule-templated syntheses is a modest step in this direction.

Table 1 Comparison of SL3 (80 mg L^{-1}) monodispersity with literature. The RSD was taken from the studies, where given, or calculated from the given mean particle diameter and standard deviation. Where multiple results are given, the range of RSD is shown

Production Process	SDA[b]	Particle Size (nm)	RSD (%)	Refs.
Biomolecule-based	Soy lecithin	496	13.1	This study
Biomolecule-based[a]	BSA/PEI	180 – 320	n/a	(Jackson et al. 2015)
Biomolecule-based	Gelatin	Non-spherical	Non-spherical	(Jia et al. 2004)
Biomolecule-based	BSA/lysozyme	50 – 200/non-spherical	No data/ non-spherical	(Coradin et al. 2003)
Biomolecule-based	Lysine/arginine	< 100	Non-spherical/ agglomerated	(Coradin et al. 2002)
Modified-Stöber	CTAB	223 – 303	5.4 – 12	(Luo et al. 2017)
Modified-Stöber	CTAB	450	4	(Stovpiaga et al. 2015)
	DTAB	700	10	
Modified-Stöber	CTAB	37 – 130	3.5 – 29	(Zhao et al. 2016)
Modified-Stöber	CTAB	100 – 1470	3.1 – 45.9	(Trofimova et al. 2013)
	DTAB	20 – 360	Non-spherical	
		471	22.4	
Stöber	Ethanolamine	122.4	6.1	(Meier et al. 2018)
Stöber	NH_3	10.2 – 236.4	1.7 – 59.8	(Park et al. 2002)
Stöber	NH_3	27 – 96	7.8 – 13.3	(Huang and Pemberton 2010)
Stöber	NH_3	15	9.3	(Wang et al. 2011)
	n-propylamine	13	11.5	
	n-butylamine	12 – 21	7.6 – 11.7	
Modified-Stöber	CTAC	21 – 111	7 – 14.8	(Lv et al. 2016)
Stöber	NH_3	100 – 870	1.2 – 18.2	(Nozawa et al. 2005)
Stöber	NH_3	51 – 769	3.5 – 12.9	(Plumeré et al. 2012)
Stöber	NH_3	245	11.4	(Nandy et al. 2014)
	Diethanolamine	186	15.6	
	Triethanolamine	82	23.2	

[a]Uses TMOS and PEI, both of which have their own associated environmental problems (*vide supra)*.

[b]SDA, structure-directing agent; BSA, bovine serum albumin; PEI, polyethyleneimine; CTAB, cetyltrimethylammonium bromide; DTAB, decyltrimethylammonium bromide; CTAC, Hexadecyltrimethylammonium chloride.

Conclusion

Biomolecules with physicochemical characteristics akin to compounds like CTAB that are traditionally used as structural directing agents (SDAs) in modified-Stöber processes, can produce small, spherical, monodisperse silica particles. Our syntheses are more environmentally sustainable than these processes. CTAB (a synthetic, amphiphilic surfactant), ethanol, and ammonium hydroxide were replaced in a modified-Stöber silica synthesis with less toxic, more sustainable equivalents: the biomolecules phosphatidylcholine (PC) or soy lecithin (SL); from a waste source, buffered water (plus soybean oil for PC), and acetate buffer, respectively. PC and SL can function as SDAs in the synthesis of spherical silica particles. Long-chain polyamines and proteins, such as silaffins and silacidins are integral to silica formation in the natural silica biomineralisation processes of organisms like diatoms. SL and PC bear close similarities to these diatom biopolymers. Furthermore, the physicochemical similarities that PC and SL have with CTAB, allows them to function as substitutes for CTAB in our synthesis. A mixture of Ostwald ripening and coalescence was shown to occur at low biomolecule concentrations, while transitioning to an Ostwald ripening dominated process at high biomolecule concentrations. Higher biomolecule concentrations also tended to increase particle size. The data show that SL gives much greater control over particle size and morphology and produces smaller, more monodisperse silica particles than using PC. This emphasises the progress our research represents in harnessing biomineralisation processes for producing small, monodisperse, spherical silica particles. The silica produced herein is among the best produced from biomolecules seen in the literature to date – it is spherical, discrete, statistically analysed, and has comparable monodispersity to silica prepared using Stöber/modified-Stöber processes. Preliminary results also show that porosity can be achieved using these biomolecule-based syntheses, although further

work is needed to optimise this. Our process is a significant step forward in evolving the traditional methods of silica manufacturing - an inherently unsustainable and environmentally damaging process - into one that is sustainable and environmentally benign. We have shown that not only can spherical silica particles be prepared using more environmentally benign and sustainable conditions along with PC and SL, but also that a much higher degree of control over the morphology and monodispersity can be achieved than has been reported previously using such systems.

Declarations

Funding

This research was funded by AMBER through Science Foundation Ireland (Grant No.: 12/RC/2278) and Glantreo Ltd.

Conflicts of interest/Competing interests

On behalf of all authors, the corresponding author states that there is no conflict of interest.

Data availability

All data included in the manuscript is available.

Acknowledgements

We wish to thank Dr John Hanrahan for useful discussions and Dr. Joe McGrath for running the BET analysis.

References

Alothman Z (2012) A Review: Fundamental Aspects of Silicate Mesoporous Materials. Materials (Basel) 5:2874–2902. https://doi.org/10.3390/ma5122874

Anderson MT, Martin JE, Odinek JG, Newcomer PP (1998) Effect of methanol concentration on CTAB micellization and on the formation of surfactant-templated silica (STS). Chem Mater 10:1490–1500. https://doi.org/10.1021/cm970240m

Banta RA, Collins TW, Curley RA, et al (2018) Nanopatterned protein-polysaccharide thin films by humidity regulated phase separation. J Colloid Interface Sci 532:. https://doi.org/10.1016/j.jcis.2018.07.109

Bebensee F, Voigts F, Maus-Friedrichs W (2008) The adsorption of oxygen and water on Ca and CaO films studied with MIES, UPS and XPS. Surf Sci 602:1622–1630. https://doi.org/10.1016/j.susc.2008.02.011

Belton D, Paine G, Patwardhan S V., Perry CC (2004) Towards an understanding of (bio)silicification: the role of amino acids and lysine oligomers in silicification. J Mater Chem 14:2231. https://doi.org/10.1039/b401882f

Büchel G, Grün M, Unger KK, et al (1998) Tailored syntheses of nanostructured silicas: Control of particle morphology, particle size and pore size. Supramol Sci 5:253–259. https://doi.org/10.1016/S0968-5677(98)00016-9

Cabezas DM, Diehl BWK, Tomás MC (2009) Sunflower lecithin: Application of a fractionation process with absolute ethanol. JAOCS, J Am Oil Chem Soc 86:189–196. https://doi.org/10.1007/s11746-008-1336-5

Cabezas DM, Diehl BWK, Tomás MC (2016) Emulsifying properties of hydrolysed and low HLB sunflower lecithin mixtures. Eur J Lipid Sci Technol 118:975–983.

https://doi.org/10.1002/ejlt.201500182

Capello C, Fischer U, Hungerbühler K (2007) What is a green solvent? A comprehensive framework for the environmental assessment of solvents. Green Chem 9:927–934. https://doi.org/10.1039/b617536h

Chen Y, Feng Y, Deveaux JG, et al (2019) Biomineralization Forming Process and Bio-inspired Nanomaterials for Biomedical Application: A Review. Minerals 9:68. https://doi.org/10.3390/min9020068

Cho C-S (2012) Design and Development of Degradable Polyethylenimines for Delivery of DNA and Small Interfering RNA: An Updated Review. ISRN Mater Sci 2012:1–24. https://doi.org/10.5402/2012/798247

Coradin T, Coupé A, Livage J (2003) Interactions of bovine serum albumin and lysozyme with sodium silicate solutions. Colloids Surfaces B Biointerfaces 29:189–196. https://doi.org/10.1016/S0927-7765(02)00208-4

Coradin T, Durupthy O, Livage J (2002) Interactions of amino-containing peptides with sodium silicate and colloidal silica: A biomimetic approach of silicification. Langmuir 18:2331–2336

Demadis KD, Pachis K, Ketsetzi A, Stathoulopoulou A (2009) Bioinspired control of colloidal silica in vitro by dual polymeric assemblies of zwitterionic phosphomethylated chitosan and polycations or polyanions. Adv Colloid Interface Sci 151:33–48. https://doi.org/10.1016/j.cis.2009.07.005

Fragou F, Moularas C, Adamska K, et al (2020) Mn(II)-Based Catalysts Supported on Nanocarbon-Coated Silica Nanoparticles for Alkene Epoxidation. ACS Appl Nano Mater 3:5583–5592. https://doi.org/10.1021/acsanm.0c00849

Galarneau A, Renard G, Mureseanu M, et al (2007) Synthesis of sponge mesoporous silicas from

lecithin/dodecylamine mixed-micelles in ethanol/water media: A route towards efficient biocatalysts. Microporous Mesoporous Mater 104:103–114. https://doi.org/10.1016/j.micromeso.2007.01.017

Gautier C, Abdoul-Aribi N, Roux C, et al (2008) Biomimetic dual templating of silica by polysaccharide/protein assemblies. Colloids Surfaces B Biointerfaces 65:140–145. https://doi.org/10.1016/j.colsurfb.2008.03.005

Gong C, Sun S, Zhang Y, et al (2019) Hierarchical nanomaterials via biomolecular self-assembly and bioinspiration for energy and environmental applications. Nanoscale 11:4147–4182. https://doi.org/10.1039/C9NR00218A

Gustus R, Gruber W, Wegewitz L, et al (2014) Decomposition of amorphous Si2C by thermal annealing. Thin Solid Films 552:232–240. https://doi.org/10.1016/j.tsf.2013.12.033

Han Y, Lu Z, Teng Z, et al (2017) Unraveling the growth mechanism of silica particles in the stöber method: In situ seeded growth model. Langmuir 33:5879–5890. https://doi.org/10.1021/acs.langmuir.7b01140

Heintze C, Formanek P, Pohl D, et al (2020) An intimate view into the silica deposition vesicles of diatoms. BMC Mater 2:11. https://doi.org/10.1186/s42833-020-00017-8

Himpsel FJ, McFeely FR, Taleb-Ibrahimi A, et al (1988) Microscopic structure of the SiO2/Si interface. Phys Rev B 38:6084–6096. https://doi.org/10.1103/PhysRevB.38.6084

Hollinger G, Himpsel FJ (1984) Probing the transition layer at the SiO 2 -Si interface using core level photoemission. Appl Phys Lett 44:93–95. https://doi.org/10.1063/1.94565

Huang Y, Pemberton JE (2010) Synthesis of uniform, spherical sub-100nm silica particles using a conceptual modification of the classic LaMer model. Colloids Surfaces A Physicochem Eng Asp 360:175–183. https://doi.org/10.1016/j.colsurfa.2010.02.031

Hyde EDER, Seyfaee A, Neville F, Moreno-Atanasio R (2016) Colloidal Silica Particle Synthesis and Future Industrial Manufacturing Pathways: A Review. Ind Eng Chem Res 55:8891–8913. https://doi.org/10.1021/acs.iecr.6b01839

Jackson E, Ferrari M, Cuestas-Ayllon C, et al (2015) Protein-Templated Biomimetic Silica Nanoparticles. Langmuir 31:3687–3695. https://doi.org/10.1021/la504978r

Jia J, Zhou X, Caruso RA, Antonietti M (2004) Synthesis of Microporous Silica Templated by Gelatin. Chem Lett 33:202–203. https://doi.org/10.1246/cl.2004.202

Keane DA, Hanrahan JP, Copley MP, et al (2010) A modified Stöber process for the production of mesoporous Sub 2 micron silica microspheres; applications in HPLC. J Porous Mater 17:145–152. https://doi.org/10.1007/s10934-009-9274-7

Kolbe F, Daus F, Geyer A, Brunner E (2020) Phosphate–Silica Interactions in Diatom Biosilica and Synthetic Composites Studied by Rotational Echo Double Resonance (REDOR) NMR Spectroscopy. Langmuir 36:4332–4338. https://doi.org/10.1021/acs.langmuir.0c00336

Kotzsch A, Gröger P, Pawolski D, et al (2017) Silicanin-1 is a conserved diatom membrane protein involved in silica biomineralization. BMC Biol 15:9–11. https://doi.org/10.1186/s12915-017-0400-8

Kröger N, Lorenz S, Brunner E, Sumper M (2014) Self-Assembly of Highly Phosphorylated Silaffins and Their Function in Biosilica Morphogenesis. Science (80-) 298:584–586. https://doi.org/10.1126/science.1076221

Kuno T, Nonoyama T, Hirao K, Kato K (2011) Influence of the charge relay effect on the silanol condensation reaction as a model for silica biomineralization. Langmuir 27:13154–13158. https://doi.org/10.1021/la202576v

Le CTM, Houri A, Balage N, et al (2019) Interaction of Small Ionic Species With Phospholipid

Membranes: The Role of Metal Coordination. Front Mater 5:. https://doi.org/10.3389/fmats.2018.00080

Lechner CC, Becker CFW (2015) Silaffins in silica biomineralization and biomimetic silica precipitation. Mar Drugs 13:5297–5333. https://doi.org/10.3390/md13085297

Lifshitz IM, Slyozov VV (1961) The kinetics of precipitation from supersaturated solid solutions. J Phys Chem Solids 19:35–50. https://doi.org/10.1016/0022-3697(61)90054-3

Lopez P, Gautier C, Livage J, Coradin T (2006) Mimicking Biogenic Silica Nanostructures Formation. Curr Nanosci 1:73–83. https://doi.org/10.2174/1573413052953156

Lorber B, Fischer F, Bailly M, et al (2012) Protein analysis by dynamic light scattering: Methods and techniques for students. Biochem Mol Biol Educ 40:372–382. https://doi.org/10.1002/bmb.20644

Lotty O, Hobbs R, O'Regan C, et al (2013) Self-seeded growth of germanium nanowires: Coalescence and ostwald ripening. Chem Mater 25:215–222. https://doi.org/10.1021/cm3032863

Luo L, Liang Y, Erichsen ES, Anwander R (2017) Monodisperse mesoporous silica nanoparticles of distinct topology. J Colloid Interface Sci 495:84–93. https://doi.org/10.1016/j.jcis.2017.01.107

Lv X, Zhang L, Xing F, Lin H (2016) Controlled synthesis of monodispersed mesoporous silica nanoparticles: Particle size tuning and formation mechanism investigation. Microporous Mesoporous Mater 225:238–244. https://doi.org/10.1016/j.micromeso.2015.12.024

Ma Y, Ardell AJ (2007) Coarsening of γ (Ni–Al solid solution) precipitates in a γ′ (Ni3Al) matrix. Acta Mater 55:4419–4427. https://doi.org/10.1016/j.actamat.2007.04.008

Mann S (2001) Biomineralization: Principles and Concepts in Bioinorganic Materials Chemistry.

Oxford University Press

Manzano M, Vallet-Regí M (2020) Mesoporous Silica Nanoparticles for Drug Delivery. Adv Funct Mater 30:1902634. https://doi.org/10.1002/adfm.201902634

Masse S, Laurent G, Chuburu F, et al (2008) Modification of the stöber process by a polyazamacrocycle leading to unusual core-shell silica nanoparticles. Langmuir 24:4026–4031. https://doi.org/10.1021/la703828v

Meier M, Ungerer J, Klinge M, Nirschl H (2018) Synthesis of nanometric silica particles via a modified Stöber synthesis route. Colloids Surfaces A Physicochem Eng Asp 538:559–564. https://doi.org/10.1016/j.colsurfa.2017.11.047

Möller K, Bein T (2016) Talented Mesoporous Silica Nanoparticles. Chem Mater acs.chemmater.6b03629. https://doi.org/10.1021/acs.chemmater.6b03629

Murai K, Higuchi M, Kuno T, Kato K (2014) Silica mineralization by a peptide template having a high charge relay effect. Chempluschem 79:531–535. https://doi.org/10.1002/cplu.201300321

Murdan S (2005) A review of pluronic lecithin organogel as a topical and transdermal drug delivery system. Hosp Pharm 12:267–270

Naderizadeh S, Athanassiou A, Bayer IS (2018) Interfacing superhydrophobic silica nanoparticle films with graphene and thermoplastic polyurethane for wear/abrasion resistance. J Colloid Interface Sci 519:285–295. https://doi.org/10.1016/j.jcis.2018.02.065

Nałęcz-Jawecki G, Grabińska-Sota E, Narkiewicz P (2003) The toxicity of cationic surfactants in four bioassays. Ecotoxicol Environ Saf 54:87–91. https://doi.org/10.1016/S0147-6513(02)00025-8

Nandy S, Kundu D, Naskar MK (2014) Synthesis of mesoporous Stöber silica nanoparticles: the

effect of secondary and tertiary alkanolamines. J Sol-Gel Sci Technol 72:49–55. https://doi.org/10.1007/s10971-014-3420-7

Nozawa K, Gailhanou H, Raison L, et al (2005) Smart Control of Monodisperse Stöber Silica Particles: Effect of Reactant Addition Rate on Growth Process. Langmuir 21:1516–1523. https://doi.org/10.1021/la048569r

Pamirsky IE, Golokhvast KS (2013) Silaffins of diatoms: From applied biotechnology to biomedicine. Mar Drugs 11:3155–3167. https://doi.org/10.3390/md11093155

Park SK, Kim K Do, Kim HT (2002) Preparation of silica nanoparticles: Determination of the optimal synthesis conditions for small and uniform particles. Colloids Surfaces A Physicochem Eng Asp 197:7–17. https://doi.org/10.1016/S0927-7757(01)00683-5

Patwardhan S V., Clarson SJ (2002) Silicification and biosilicification. Silicon Chem 207–214

Patwardhan S V., Clarson SJ, Perry CC (2005) On the role(s) of additives in bioinspired silicification. Chem Commun 1113. https://doi.org/10.1039/b416926c

Patwardhan S V, Staniland SS (2019) Biomineralisation: how Nature makes nanomaterials. In: Green Nanomaterials: From bioinspired synthesis to sustainable manufacturing of inorganic nanomaterials. IOP Publishing

Perrett S, Buell AK, Knowles TPJ (eds) (2019) Biological and Bio-inspired Nanomaterials. Springer Singapore, Singapore

Plumeré N, Ruff A, Speiser B, et al (2012) Stöber silica particles as basis for redox modifications: Particle shape, size, polydispersity, and porosity. J Colloid Interface Sci 368:208–219. https://doi.org/10.1016/j.jcis.2011.10.070

Post P, Wurlitzer L, Maus-Friedrichs W, Weber A (2018) Characterization and Applications of Nanoparticles Modified in-Flight with Silica or Silica-Organic Coatings. Nanomaterials

8:530. https://doi.org/10.3390/nano8070530

Prasomsri T, Jiao W, Weng SZ, Garcia Martinez J (2015) Mesostructured zeolites: bridging the gap between zeolites and MCM-41. Chem Commun 51:8900–8911. https://doi.org/10.1039/C4CC10391B

Rahman IA, Padavettan V (2012) Synthesis of Silica nanoparticles by Sol-Gel: Size-dependent properties, surface modification, and applications in silica-polymer nanocompositesa review. J Nanomater 2012:. https://doi.org/10.1155/2012/132424

Ramanathan R, Campbell JL, Soni SK, et al (2011) Cationic Amino Acids Specific Biomimetic Silicification in Ionic Liquid: A Quest to Understand the Formation of 3-D Structures in Diatoms. PLoS One 6:e17707. https://doi.org/10.1371/journal.pone.0017707

Sadri R, Hosseini M, Kazi SN, et al (2017) A bio-based, facile approach for the preparation of covalently functionalized carbon nanotubes aqueous suspensions and their potential as heat transfer fluids. J Colloid Interface Sci 504:115–123. https://doi.org/10.1016/j.jcis.2017.03.051

Santos J, Calero N, Trujillo-Cayado LA, et al (2017) Assessing differences between Ostwald ripening and coalescence by rheology, laser diffraction and multiple light scattering. Colloids Surfaces B Biointerfaces 159:405–411. https://doi.org/10.1016/j.colsurfb.2017.08.015

Shaikh I, Jadhav K, Gide P, et al (2006) Topical Delivery of Aceclofenac from Lecithin Organogels: Preformulation Study. Curr Drug Deliv 3:417–427. https://doi.org/10.2174/156720106778559010

Slowing II, Vivero-Escoto JL, Trewyn BG, Lin VS-Y (2010) Mesoporous silica nanoparticles: structural design and applications. J Mater Chem 20:7924. https://doi.org/10.1039/c0jm00554a

Sobańska AW (2020) Emerging or Underestimated Silica-Based Stationary Phases in Liquid Chromatography. Crit Rev Anal Chem 1–25. https://doi.org/10.1080/10408347.2020.1760782

Soleimani M, Rutten L, Maddala SP, et al (2020) Modifying the thickness, pore size, and composition of diatom frustule in Pinnularia sp. with Al3+ ions. Sci Rep 10:19498. https://doi.org/10.1038/s41598-020-76318-5

Sprenger KG, Prakash A, Drobny G, Pfaendtner J (2018) Investigating the Role of Phosphorylation in the Binding of Silaffin Peptide R5 to Silica with Molecular Dynamics Simulations. Langmuir 34:1199–1207. https://doi.org/10.1021/acs.langmuir.7b02868

Stovpiaga EY, Kurdyukov DA, Kukushkina YA, et al (2015) Monodisperse spherical silica particles with controlled-varied diameter of micro- and mesopores. Glas Phys Chem 41:316–323. https://doi.org/10.1134/S1087659615030153

Sumper M, Kröger N (2004) Silica formation in diatoms: The function of long-chain polyamines and silaffins. J Mater Chem 14:2059–2065. https://doi.org/10.1039/b401028k

Sumper M, Lorenz S, Brunner E (2003) Biomimetic Control of Size in the Polyamine-Directed Formation of Silica Nanospheres. Angew Chemie - Int Ed 42:5192–5195. https://doi.org/10.1002/anie.200352212

Tengjisi, Hui Y, Yang G, et al (2021) Biomimetic core–shell silica nanoparticles using a dual-functional peptide. J Colloid Interface Sci 581:185–194. https://doi.org/10.1016/j.jcis.2020.07.107

Thommes M (2010) Physical Adsorption Characterization of Nanoporous Materials. Chemie Ing Tech 82:1059–1073. https://doi.org/10.1002/cite.201000064

Tilburey GE, Blundell TJ, Argent SP, Perry CC (2019) Azamacrocycles and tertiary amines can

be used to form size tuneable hollow structures or monodisperse oxide nanoparticles depending on the “M” source. Dalt Trans 48:15470–15479. https://doi.org/10.1039/c9dt02080b

Trinh TT, Jansen APJ, Van Santen RA (2006) Mechanism of oligomerization reactions of silica. J Phys Chem B 110:23099–23106. https://doi.org/10.1021/jp063670l

Trofimova EY, Kurdyukov DA, Yakovlev SA, et al (2013) Monodisperse spherical mesoporous silica particles: Fast synthesis procedure and fabrication of photonic-crystal films. Nanotechnology 24:. https://doi.org/10.1088/0957-4484/24/15/155601

Wagner C (1961) Theorie der Alterung von Niederschlägen durch Umlösen (Ostwald-Reifung). Berichte der Bunsengesellschaft für Phys Chemie 65:581–591. https://doi.org/10.1002/BBPC.19610650704

Wallace AF, DeYoreo JJ, Dove PM (2009) Kinetics of silica nucleation on carboxyl- and amine-terminated surfaces: Insights for biomineralization. J Am Chem Soc 131:5244–5250. https://doi.org/10.1021/ja809486b

Wang J, Sugawara-Narutaki A, Fukao M, et al (2011) Two-phase synthesis of monodisperse silica nanospheres with amines or ammonia catalyst and their controlled self-assembly. ACS Appl Mater Interfaces 3:1538–1544. https://doi.org/10.1021/am200104m

Wang Q, Zhang C, Shen G, et al (2014) Fluorescent carbon dots as an efficient siRNA nanocarrier for its interference therapy in gastric cancer cells. J Nanobiotechnology 12:58. https://doi.org/10.1186/s12951-014-0058-0

Wenzl S, Hett R, Richthammer P, Sumper M (2008) Silacidins: Highly acidic phosphopeptides from diatom shells assist in silica precipitation in vitro. Angew Chemie - Int Ed 47:1729–1732. https://doi.org/10.1002/anie.200704994

Wysokowski M, Jesionowski T, Ehrlich H (2018) Biosilica as a source for inspiration in biological materials science. Am Mineral 103:665–691. https://doi.org/10.2138/am-2018-6429

Xia L (2014) The Structure Evolution of Biomimetic Silica Directed by Poly(L-lysine). Adv Mater Res 926–930:292–295. https://doi.org/10.4028/www.scientific.net/AMR.926-930.292

Yang H-W, Kang N, Myung S-T, et al (2018) Exceptional Effect of Benzene in Uniform Carbon Coating of SiO x Nanocomposite for High-Performance Li-Ion Batteries. J Electrochem Soc 165:A1247–A1253. https://doi.org/10.1149/2.0291807jes

Yi Z, Dumée LF, Garvey CJ, et al (2015) A New Insight into Growth Mechanism and Kinetics of Mesoporous Silica Nanoparticles by in Situ Small Angle X-ray Scattering. Langmuir 31:8478–8487. https://doi.org/10.1021/acs.langmuir.5b01637

Zhao Z, Wang X, Jiao Y, et al (2016) Facile, low-cost, and scalable fabrication of particle size and pore structure tuneable monodisperse mesoporous silica nanospheres as supports for advanced solid acid catalysts. RSC Adv 6:9072–9081. https://doi.org/10.1039/c5ra26432d